Molecular dynamics simulations of yttrium-stabilized zirconia

1995 J. Phys.: Condens. Matter 7 1255

(http://iopscience.iop.org/0953-8984/7/7/007)

J. Phys.: Condens. Matter 7 (1995) 1255–1271. Printed in the UK

Molecular dynamics simulations of yttrium-stabilized zirconia

Xiaoyun Li† and Bjørn Hafskjold‡

Department of Physical Chemistry, University of Trondheim, The Norwegian Institute of Technology, N-7034 Trondheim, Norway

Received 29 June 1994, in final form 14 November 1994

Abstract. The electric conductivity of yttrium-stabilized zirconia exhibits a maximum as a function of dopant (Y^{3+}) cation concentration in isothermal and isobaric conditions. In order to improve the conductivity of this important solid electrolyte, it is essential to understand the ion transport mechanisms at the molecular level. This was investigated by the molecular dynamics simulations method in the present study.

The composition dependency of the electric conductivity was found to agree qualitatively with experimental data. The conductivity was found to depend on the dopant Y^{3+} distribution. The O^{2-}–O^{2-} radial distribution function showed that oxygen ions were displaced about 0.37 Å towards O^{2-} vacancies. The radial distribution functions of cations showed that the local structural environment of Y^{3+} ions was more disordered than that of the Zr^{4+} ions. Oxygen vacancies were found to be nearest neighbours of Y^{3+} ions. The Y^{3+}–Y^{3+} neighbour clusters trapped more O^{2-} vacancies than did isolated Y^{3+} ions, and this tendency increased with increasing Y_2O_3 concentration in ZrO_2 because more and larger Y^{3+}–Y^{3+} clusters were formed. We suggest that this is responsible for the observed isothermal conductivity decrease at high Y_2O_3 contents in the yttrium-stabilized zirconia.

1. Introduction

Yttrium-stabilized zirconia has been used as a solid electrolyte in high-temperature solid oxide fuel cells and oxygen sensors, owing to its outstanding electrical and mechanical properties. In the last three decades, a vast amount of work has been done to investigate the behaviour of the stabilized zirconias (Vashishta *et al* 1979, Heuer and Hobbs 1981, Claussen *et al* 1984, Poulsen *et al* 1985, Sōmiya *et al* 1988, Takahashi 1989, Stoneham 1989).

The crystal structure of the fully stabilized zirconia is of the cubic fluorite type, where the cations form a close-packed FCC lattice and oxygen ions occupy tetrahedral sites. Some oxygen sites are vacant according to the vacancy concentration caused by the dopant Y_2O_3. According to the phase diagram of the Y_2O_3–ZrO_2 system (Stubican 1988), it takes about 8 mol% Y_2O_3 to stabilize the cubic ZrO_2 (called fully stabilized zirconia). In the range of 2–8 mol% Y_2O_3, both tetragonal and cubic phases are present (called partially stabilized zirconia). These structures are stable only at temperatures above 600 °C.

It has been known for a long time that the isothermal ionic conductivity exhibits a maximum for a given dopant concentration in all the stabilized zirconias. The maximum is located near the zirconia-rich boundary of the cubic phase. For instance, the maximum conductivity occurs around 8–9 mol% in the Y_2O_3 stabilized zirconia, in the vicinity of the partially and fully stabilized two-phase region.

† Current address: SINTEF Industrial Mathematics, N-7034 Trondheim, Norway.

‡ To whom correspondence should be addressed.

0953-8984/95/071255+17$19.50

Atomistic simulations of the calcium-stabilized zirconia suggest that the formation of ordered phases or microdomains plays an important role for the observed fall in the electric conductivity at high CaO content (Dwivedi and Cormack 1989). Atomistic calculations (Catlow 1984) and Monte Carlo simulations (Murch *et al* 1986) of a similar system, Y_2O_3–CeO_2, have attributed the conductivity drop after the maximum to the increasing number of defect clusters. For the yttrium-stabilized zirconia, no conclusive explanation of the conductivity maximum can be given at present. Hull *et al* (1988) concluded that the increasing number of defect clusters causes the conductivity fall at high Y_2O_3 content. Other investigations suggest that the defect structure may be more complex (Catlow *et al* 1986a, b).

In the fully stabilized Y_2O_3–ZrO_2 system, the defect concentration is above 8 mol% and there are substantial interactions between defects. Simple descriptions based on point defects in normal ionic solids are therefore of limited value for the understanding of the ion transport processes in the material.

To our knowledge, MD simulations have never been made on stabilized zirconias. It is generally believed that the electronic structures of the ions and the ionic polarization are important in the stabilized zirconias. It has been doubted that simple potential models omitting the electronic polarizability of the ions (rigid-ion models), are sufficiently realistic to represent the stabilized zirconias. Our simulation results on the Y_2O_3–ZrO_2 system show that by choosing appropriate sets of potential parameters from the literature, a rigid-ion potential model can qualitatively reproduce the isothermal ionic conductivity maximum around 8 mol% Y_2O_3 at low temperatures.

It has been suspected that the dopant cation distribution is very important in determining the ion transport rate. It is, however, still impossible to experimentally detect the cation distribution and find its influence on the ionic conductivity. In this study, the oxygen diffusion coefficient is computed for different dopant cation Y^{3+} distributions and temperatures (see also Li 1993). We show that the conductivity depends on the dopant distribution and decreases with increasing number of the nearest-Y^{3+}–Y^{3+}-neighbour pairs.

The rest of the paper is arranged as follows. Section 2 describes the simulated systems and the different sets of potential parameters used. The oxygen transport properties are discussed in section 3. In section 4, the radial distribution functions of ions and the defect structure in the material are discussed and analysed. Finally, our conclusions from the present study are given in section 5.

2. The model systems

Compositions of 4.85, 8.00, 11.34, 14.89, and 20.00 mol% Y_2O_3 in ZrO_2 were investigated. The size of the basic simulation box was $3a \times 3b \times 3c$, where $a = b = c$ is the lattice constant of the cubic crystallographic unit cell. For pure ZrO_2, the box contained 108 cations and 216 anions. In the Y_2O_3–ZrO_2 system, every two Y^{3+} dopant ions create one oxygen vacancy.

The lattice constant determined by Ingel and Lewis (1986) at room temperature was taken as basis, and $\alpha_a = 1.0 \times 10^{-5}$ K^{-1} was used as the thermal expansion coefficient for all the compositions studied.

In order to study the effect of the dopant ion distribution, we chose two sets of positions:

(1) The Y^{3+} ions were assigned randomly to cation sites. This Y^{3+} distribution is denoted by YI in the following.

(2) The Y^{3+} ions were assigned manually in such a way that there were more nearest-neighbour or next-nearest-neighbour Y^{3+}–Y^{3+} pairs than in the YI distribution. This Y^{3+} distribution is referred to as YII in this study.

Table 1 gives the numbers of nearest-neighbour (NN) and next-nearest-neighbour (NNN) Y^{3+}–Y^{3+} pairs for the two Y^{3+} distributions. To simplify the notation, we shall in the following use Y–Y to represent the Y^{3+}–Y^{3+} pair. Similarly, the notations O–O, Y–O, and Zr–O will also be used.

Table 1. Numbers of nearest- and next-nearest Y^{3+}–Y^{3+} pairs for Y^{3+} distributions YI and YII.

Mol% Y_2O_3	No of NN Y^{3+}–Y^{3+} pairs		No of NNN Y^{3+}–Y^{3+} pairs	
	YI	YII	YI	YII
4.85	1	5	0	2
8.00	1	9	6	8
11.34	17	20	7	11
14.89	38	4	8	81
20.00	38	54	81	72

Oxygen vacancies were assigned randomly at the start of each series of simulations. The high-temperature simulations were always performed first in order to get a more representative distribution of oxygen vacancies. For most of the simulated systems, three temperatures, namely 900 K, 1200 K, and 1500 K were studied.

The Verlet neighbour list method (Allen and Tildesley 1987), the Beeman's algorithm (Beeman 1976), and the Ewald summation method for calculating the Coulomb interactions (Fincham 1982) were applied. The timestep was $\Delta t = 5 \times 10^{-15}$ seconds in most of the simulations. The potential cut-off distance was $R_{cut} = 6$ Å for short-range interaction, and for the real part of the Ewald summation.

Both Y^{3+} and Zr^{4+} are transition metal ions. The ionic polarizability is supposed to be important in simulations of the Y_2O_3–ZrO_3 system. The available potential models for the Y_2O_3–ZrO_2 system are all described by the shell model. Due to limited computer resources, and to test the validity of a rigid-ion model, we used the Born–Mayer–Huggins form given by equation (1).

$$V_{ij}(r) = \frac{Z_i Z_j e^2}{4\pi\epsilon_0 r} + A_{ij} \exp\left(-\frac{r}{\rho_{ij}}\right) - \frac{C_{ij}}{r^6}. \tag{1}$$

For the Y–O interaction, we found only one set of potential parameters, derived by Butler *et al* (1981) from an electron-gas procedure, which was used in their defect energy calculations of the Y_2O_3–ZrO_2 system. The cation–cation interactions were assumed to be purely Coulombic.

For the Zr–O and O–O interaction, there were three sets of potential parameters available:

(1) Potential parameters employed by Butler *et al* (1981) in atomistic calculations of the Y_2O_3–ZrO_2 system.

(2) Potential parameters derived by Cormack and Catlow (1985) according to the properties of the tetrahedral ZrO_2.

(3) Potential parameters employed by Dwivedi and Cormack (1989) in atomistic calculations of the CaO–ZrO_2 system.

Table 2. Potential parameters for the yttrium-stabilized zirconia. The sources are: B: Butler *et al* 1981. C&C: Cormack and Catlow 1985. D&C: Dwivedi and Cormack 1989.

Interaction	A_{ij} (eV)	ρ_{ij} (Å)	C_{ij} (eV Å^6)	Source
Y^{3+}–O^{2-} (PI, PII, PIII)	826.744	0.355 87	0.0	B
Zr^{4+}–O^{2-} (PI)	1067.0	0.3764	2.0	B
Zr^{4+}–O^{2-} (PII)	1453.8	0.35	0.0	C&C
Zr^{4+}–O^{2-} (PIII)	985.869	0.376	0.0	D&C
O^{2-}–O^{2-} (PI)	22 764.3	0.149	112.0	B
O^{2-}–O^{2-} (PII, PIII)	22 764.3	0.149	27.89	C&C
Y^{3+}–Y^{3+} (PI, PII, PIII)	0.0	N/A	0.0	
Y^{3+}–Zr^{4+} (PI, PII, PIII)	0.0	N/A	0.0	
Zr^{4+}–Zr^{4+} (PI, PII, PIII)	0.0	N/A	0.0	

The above three sets of potential parameters are here denoted PI, PII, and PIII, respectively, and they are listed in table 2.

Short test runs showed that the model system was unstable when employing set PI. This is because the O–O interaction in the model is too attractive at short distances, and the model system will collapse when two oxygen ions are too close to each other. Model systems applying sets PII and PIII could, however, develop normally, and these parameters were then employed in this work.

The lattice energies obtained for the 8.00 mol% Y_2O_3–ZrO_2 system at 900 K were $-10\,105.2$ and $-10\,020.9$ kJ mol^{-1} with PII and PIII, respectively. The lattice energy for the pure cubic or tetrahedral ZrO_2 is about $-11\,000$ kJ mol^{-1} from the different atomistic calculations (Mackrodt and Woodrow 1986, Bingham *et al* 1989). The close agreement between our simulated lattice energies and the literature data indicates that the simulation code and the basic input structure of the material are correct.

During the test simulations, the lattice parameters as determined from the cation positions were found to fluctuate around the input lattice parameters. The cations vibrated around their normal sites. This gave zero diffusion coefficient for the cations, while the oxygen ions had a noticeable diffusion rate. Encouraged by these results, we began a more detailed study of the Y_2O_3–ZrO_2 system by employing parameter sets PII and PIII.

The model systems were found to be stable, except at 20.00 mol% Y_2O_3. At this high vacancy concentration, the lattice parameters as determined from cation positions differ in different directions, implying that substantial cation displacement is involved. Occasionally, the total energy of the system was not conserved, i.e. the temperature would suddenly increase by several hundred degrees during the simulation. The results for the highest Y_2O_3 and vacancy concentration are therefore less reliable than the others.

3. The oxygen diffusion coefficient and ionic conductivity

The oxygen diffusion coefficient was computed by the Einstein formula

$$\langle \Delta r(t)^2 \rangle = B + 6D^t t \tag{2}$$

where $\langle \Delta r(t)^2 \rangle$ is the mean square displacement of an oxygen ion, B is a constant, t is time, and D^t is the tracer diffusion coefficient. From the slopes of the $\langle \Delta r(t)^2 \rangle$ versus t curves, the sodium diffusion coefficient was determined at three temperatures by employing potentials PII and PIII. The results are shown as D^t versus $1/T$ plots in figures 1(a) and (b) for potential PII and PIII, respectively. Since the potential models used here are very rough,

and the Y^{3+} distribution in the experimental system is unknown, a detailed comparison with experimental data seems inappropriate. There is, however, a qualitative agreement with measured tracer diffusion coefficients (Oishi and Ando 1985), as shown in the figure.

We found that the different sets of potential parameters result in very different tracer diffusion coefficients. Although most of the D^t versus $1/T$ curves are approximately linear, the slopes of the curves are somewhat different for the two sets of potential parameters. From the results of earlier experimental studies, it is known that the ionic conductivity drops when the Y_2O_3 content increases from 8 to 20 mol%. The conductivity drop is accompanied by an increase in the activation energy from about 0.7 to 1.1 eV over the same composition range (Hohnke 1979, 1981). Although our tracer diffusion data give activation energies between 0.2 and 0.8 eV, they show the increasing trend with increasing Y_2O_3 concentration in line with the experimental observations.

The tracer self-diffusion coefficient D^t can be related to the DC conductivity $\sigma(0)$ by:

$$\sigma(0) = \frac{Z^2\rho}{k_B T}\frac{D^t}{H_R} \tag{3}$$

where Z and ρ are the ionic charge and number density of the conducting ions, respectively, and H_R is the Haven ratio.

One of the aims of our simulations was to study the isothermal conductivity of the Y_2O_3–ZrO_2 system. To make a rough estimate, we converted our computed oxygen diffusion coefficients into DC conductivities by choosing $H_R = 0.65$ in the temperature and composition ranges studied. This is the ideal Haven ratio calculated from the cubic structure with vacancy diffusion mechanism at very low vacancy concentration. However, the vacancy concentration is normally very high in the stabilized zirconias. Since the experimental H_R-values for the CaO-stabilized ZrO_2, and tetrahedral ZrO_2 are all 0.65 (Simpson and Carter 1966, Park and Olander 1991), we do not think our estimation of the H_R-value for the Y_2O_3–ZrO_2 system could be very wrong. The simulated data at different temperatures were extrapolated or interpolated to exactly 900, 1200 and 1500 K.

The isothermal ionic conductivities for the YI distribution are plotted in figures 2(a) and (b). The conductivity data measured by Casselton (1970) are also shown in the figure. When the temperature is low, both PII and PIII lead to conductivity maxima as function of composition. The conductivity maximum occurs at about 11 mol% Y_2O_3 for PII and 8 mol% Y_2O_3 for PIII at about 900 K.

For potential PII, the isothermal conductivity increases with increasing Y_2O_3 content at high temperatures. Although the absolute value of the conductivity simulated by PIII is higher than the measured one, the isothermal conductivity curves resemble in this case the experimental curves.

Figure 3 shows the isothermal conductivity plots for the YI and YII distributions. At 900 K, most of the compositions give lower conductivities with YII distribution than with YI distribution. The measured diffusion coefficient and ionic conductivity have been reported to depend on the sample's thermal history (El Barhmi *et al* 1988). Our results confirm that the Y^{3+} distribution influences the diffusion coefficient at low temperatures.

From pure statistical calculations, if x is the fraction of randomly distributed dopant Y^{3+} ions in the Y_2O_3–ZrO_2 system, then the probability of finding an isolated Y^{3+} ion is $(1-x)^{18}$ (Nowick 1984). When the dopant concentration is high, almost all the Y^{3+} ions have other Y^{3+} ions in NN and/or NNN positions. This suggests that the observed isothermal conductivity decrease at higher Y^{3+} concentrations may be related to the increasing number of Y–Y neighbour pairs.

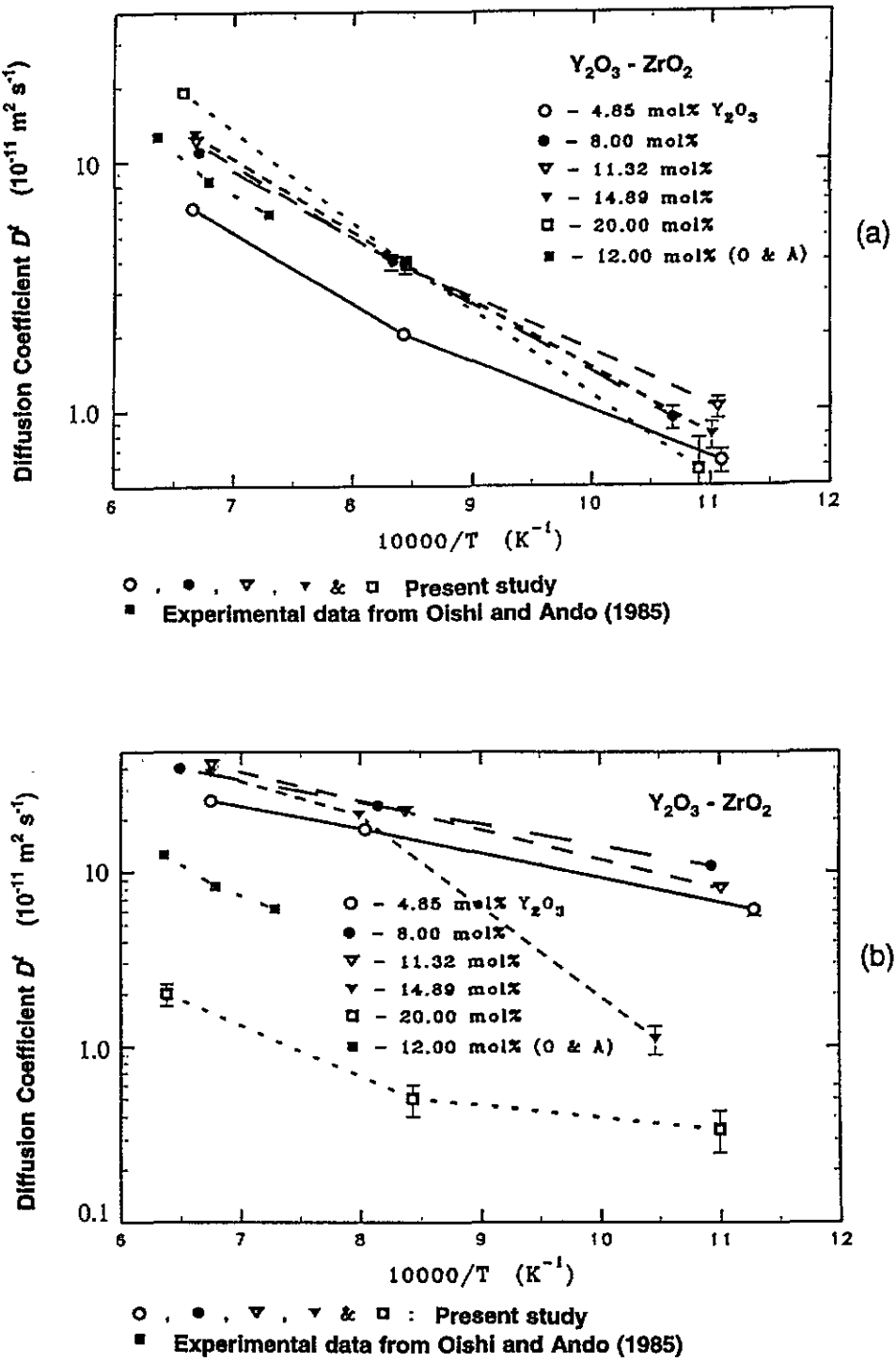

Figure 1. Temperature dependence of the oxygen diffusion coefficient. (a) With YI and PII. (b) With YI and PIII.

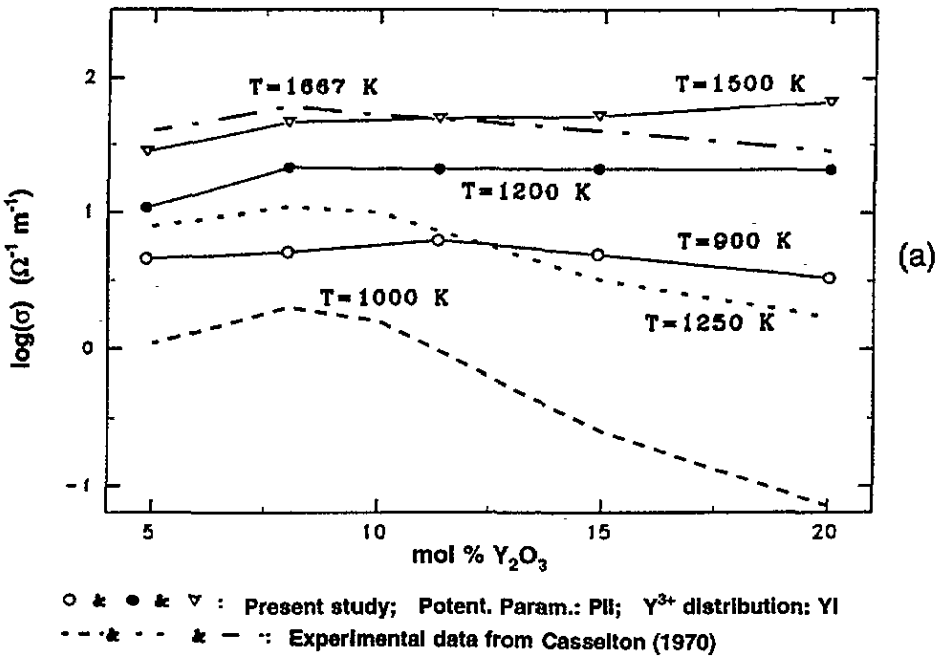

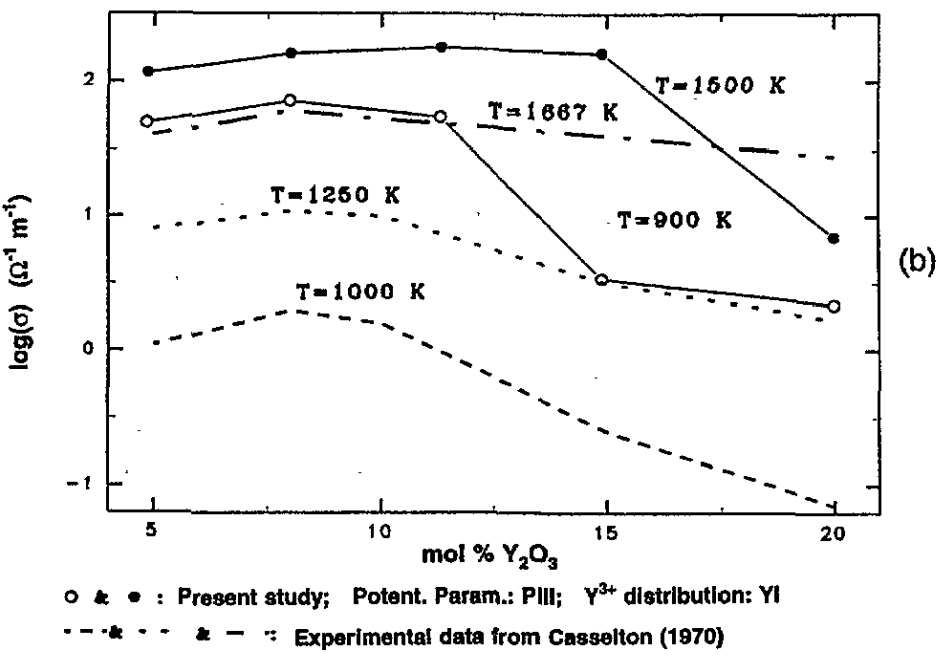

Figure 2. *Isothermal ionic conductivities converted from the oxygen diffusion coefficients for* the simulated Y_2O_3–ZrO_2 system. (a) With YI and PII. (b) With YI and PIII.

The data listed in table 1 show that at compositions 4.85, 8.00, and 11.34 mol% Y_2O_3, there are more nearest-neighbour (NN) and next-nearest-neighbour (NNN) Y–Y pairs in the

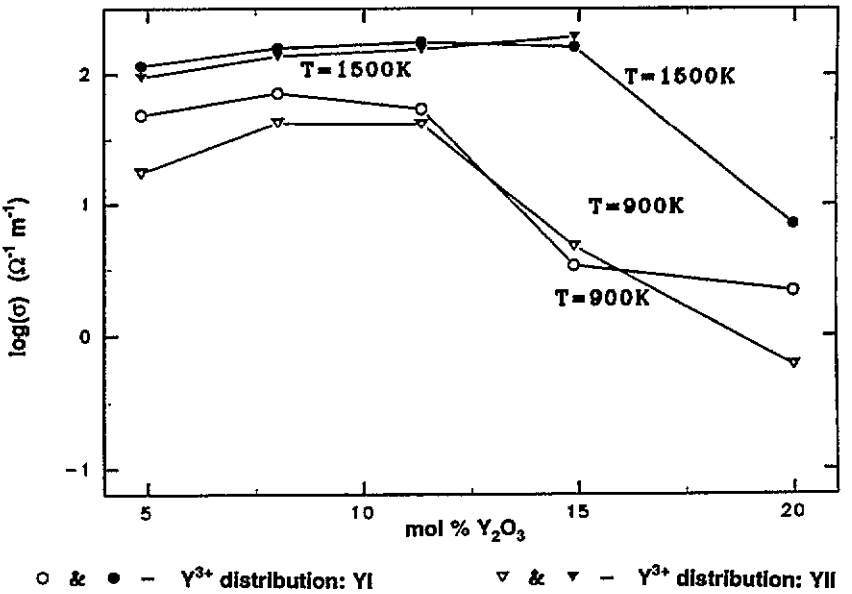

Figure 3. Isothermal ionic conductivities for the simulated Y_2O_3–ZrO_2 system with YI and YII distributions. Potential parameters: PIII.

YII distribution than in YI. At 14.89 mol% Y_2O_3, the YII distribution contains more NNN Y–Y pairs, but fewer NN Y–Y pairs. At 20.00 mol% Y_2O_3, the YII distribution contains more NN Y–Y pairs, but slightly fewer NNN Y–Y pairs. At about 900 K, the ionic conductivity at each composition is lower in YII than in YI, except at 14.89 mol% Y_2O_3. This suggests that NN Y–Y pairs can trap more oxygen vacancies than isolated Y^{3+} ions can. Here an isolated Y^{3+} ion is defined as one with no other Y^{3+} ions in NN or NNN positions. The effect of the NNN Y–Y pair is not very clear from figure 3. In section 4, we will discuss more thoroughly the effect of NNN Y–Y clusters on the trapping of oxygen vacancies, especially at high Y_2O_3 content.

When the temperature is increased, more oxygen ions become mobile. Figure 3 shows that the conductivity difference between YI and YII is small at high temperature, indicating that the influence from the Y–Y neighbour pairs to the conductivity is weakened at high temperatures. Thus we can conclude that Y–Y neighbour pairs can trap oxygen vacancies, and the ability of trapping oxygen vacancies is degraded with increasing temperature.

Of course, the Y–Y neighbour pairs can form even bigger clusters at high Y_2O_3 contents, e.g., 2, 3 and more NN and/or NNN Y–Y pairs together. This will certainly influence the mobility of oxygen vacancies, i.e. the ionic conductivity.

Despite the fact that the potential parameters used in our simulations were taken directly from the corresponding shell model and no optimization of the parameters was made for the rigid-ion model, the qualitative agreement between the computed and experimental data is good. In fact, even with the shell model, calculations based on simple theories could not reproduce the experimental data completely for a similar system (Catlow 1984). We expect that an optimized set of potential parameters for the rigid-ion model will improve the MD simulation results for the Y_2O_3–ZrO_2 system.

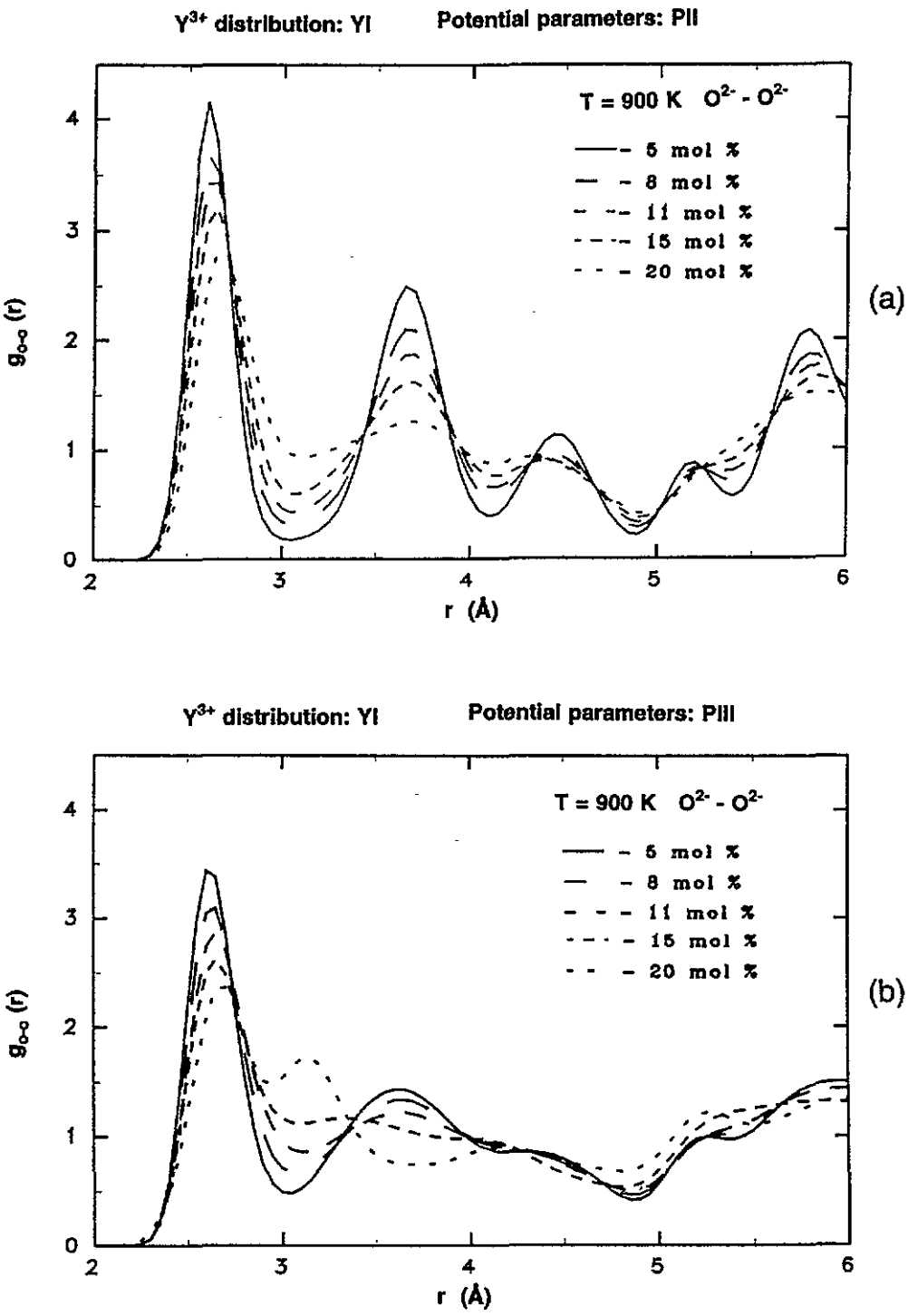

Figure 4. Radial distribution functions of oxygen ions with YI distribution. $T = 900$ K. (a) Potential PII. (b) Potential PIII.

4. Radial distribution functions

4.1. Radial distribution function of oxygen ions

The O–O radial distribution functions for the five compositions, with YI distribution, at $T = 900$ K, and for potential parameter sets PII and PIII are shown in figure 4. To simplify the notation in the graphs below, the mol% of Y_2O_3 is rounded off to the nearest integer number. At low Y_2O_3 concentrations, the $g_{O-O}(r)$ curves are sharply peaked at $r \simeq 2.6$ Å and 3.7 Å for both PII and PIII. With increasing Y_2O_3 content, the $g_{O-O}(r)$ curves become less structured, and the heights of all the peaks are reduced. The first peak at $r \simeq 2.6$ Å, shifts to higher r-values when the Y_2O_3 concentration is increased. The second peak at $r \simeq 3.7$ Å, reduces its height dramatically, while the minimum $g_{O-O}(r)$-value between the first and second peaks increases with increasing Y_2O_3 concentration. For potential PIII, a substantial change in the $g_{O-O}(r)$ curve is observed at 20.00 mol% Y_2O_3, i.e. the second peak has moved to $r \simeq 3.15$ Å.

To explain the observed features of the $g_{O-O}(r)$, we start from the basic structure of the Y_2O_3–ZrO_2 system. The nearest- and next-nearest-O–O-neighbour distances are $a/2$ and $a/\sqrt{2}$, respectively, in the cubic fluorite structure, where a is the lattice constant of the cubic structure. Provided the lattice structure is ideal, the first peak should be located at 2.58 Å and 2.6 Å for the 4.85 and 20.00 mol% Y_2O_3–ZrO_2 systems, respectively.

Atomistic calculations (Cormack 1986) have shown that around each oxygen vacancy in the stabilized zirconias, three of the nearest oxygen neighbours will displace or relax towards the vacancy, the next-nearest neighbours in the same cube will move away from the vacancy. (Figure 5 gives a 2D illustration of an oxygen vacancy and its surrounding oxygen neighbours.)

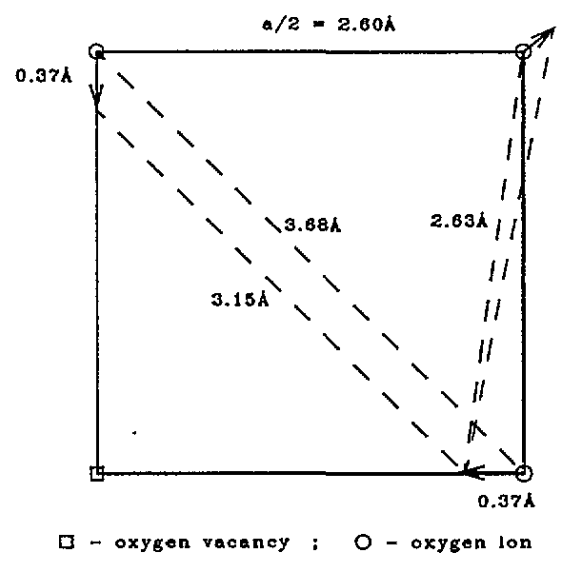

Figure 5. Illustration of an oxygen vacancy and its surrounding oxygen neighbours in a cubic fluorite structure.

If we suppose that the peak at $r \simeq 3.15$ Å at 20.00 mol% Y_2O_3 corresponds to the distance between two relaxed oxygen ions, we find the oxygen displacement to be 0.37 Å. The distance between an oxygen relaxing towards a vacancy and an oxygen moving away from a vacancy should therefore be larger than 2.63 Å as shown in figure 5.

A larger fraction of the oxygen ions will be displaced from their ideal sites at higher Y_2O_3 concentrations. As a consequence, the second peak of the $g_{O-O}(r)$ curve will move to the left, and the first peak will move to the right with increasing Y_2O_3 content. Figure 4 agrees very well with these expectations. The calculated magnitude of oxygen displacement towards vacancies, i.e. 0.37 Å, also agrees very well with the published values (Morinaga *et al* 1979, Catlow *et al* 1986a, b).

The $g_{O-O}(r)$ curves simulated at other temperatures show that the vibrational amplitude of oxygen ions increases with increasing temperature, but the locations of the peaks are essentially temperature independent.

4.2. Radial distribution functions of the cations

In the ideal fluorite structure, the cation–oxygen distances should be $(a\sqrt{3})/4$ and $(a\sqrt{11})/4$ for the nearest and next-nearest neighbours, respectively. The cation–cation nearest-neighbour distance should be $a/\sqrt{2}$, again a is the lattice constant. Figure 6 shows the Zr^{4+}-neighbour and Y^{3+}-neighbour (neighbour = O^{2-}, Zr^{4+}, or Y^{3+}) radial distribution functions with YI, PIII, and $T = 900$ K. At low Y_2O_3 content, the first three peaks of the $g(r)$ curves are centred roughly at 2.25, 3.7 and 4.3 Å. As expected, these peaks correspond to the cation–oxygen first-neighbour, cation–cation first- and cation–oxygen second-neighbour distances, respectively. The cation radial distribution function at other temperatures shows that the positions of the peaks in the $g(r)$ curves do not change very much with increasing temperature.

To study the local structural environments of cations, we will concentrate on the first peaks of the cation radial distribution functions, i.e. the nearest Y–O and Zr–O distances. The $g_{cat-O}(r)$ curves obtained from potential PII and PIII at 8.00 and 14.89 mol% Y_2O_3 are shown in figures 7(a) and (b). First we notice that the main distance between the Y–O pair is shorter than that between the Zr–O pair. With increasing Y_2O_3 content, the main peaks move to the left in both the $g_{Y-O}(r)$ and $g_{Zr-O}(r)$ curves. But the changes in the $g_{Y-O}(r)$ are more pronounced. In section 4.1, we have calculated the oxygen displacement towards vacancies to be 0.37 Å. This will reduce the cation–oxygen (relaxed) distance to 2.07 Å at 14.89 mol% Y_2O_3 and 900 K, which agrees very well with the trend shown in figure 7.

Figure 7 also shows that the $g_{Zr-O}(r)$ curve is sharper than the $g_{Y-O}(r)$ curve, indicating that the local structural environment of Y^{3+} ions is more disordered than that of the Zr^{4+} ions.

The average coordination numbers of the cations were obtained by computing the areas under the first peaks of the $g_{cat-O}(r)$ curves. The upper integration limit was taken where the $g(r)$ is minimal, in the vicinity of $r \simeq 3.2$ Å. At each composition, there is an ideal coordination number of cations calculated from the average vacancy concentration. In figure 8, we have plotted the average coordination numbers of Y^{3+} and Zr^{4+} ions obtained from potential PII and PIII. The ideal coordination numbers of cations are indicated by dashed lines in the plots. Although the potentials PII and PIII give some differences, they have a common feature, that is, the coordination number of Y^{3+} ions is smaller than the ones of Zr^{4+} ions in most of the cases. In other words, there are more oxygen vacancies near Y^{3+} ions than near Zr^{4+} ions. We interpret this as an indication that vacancies are more likely to be trapped by Y^{3+} ions, causing the conductivity decrease. The result agrees with the conductivity data, which show that more Y–Y neighbour pairs result in lower conductivity.

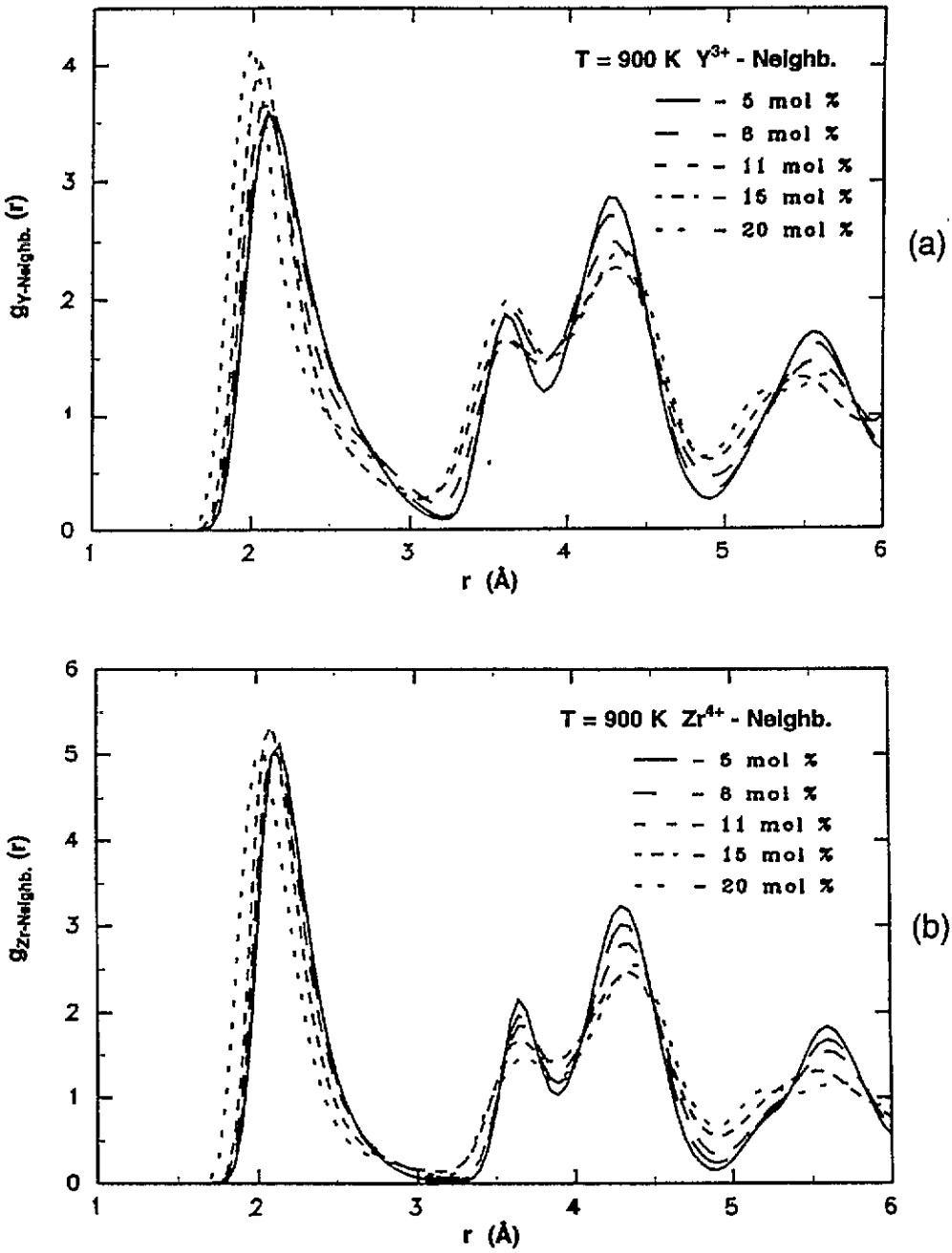

Figure 6. Radial distribution functions of Y^{3+} and Zr^{4+} ions. Conditions: YI, PIII and $T = 900$ K.

In figure 8(b), the coordination numbers of both Y^{3+} and Zr^{4+} ions are much smaller than the ideal coordination numbers at high Y_2O_3 contents. This can only be explained by displacements of cations somewhat away from their ideal sites, in addition to oxygen

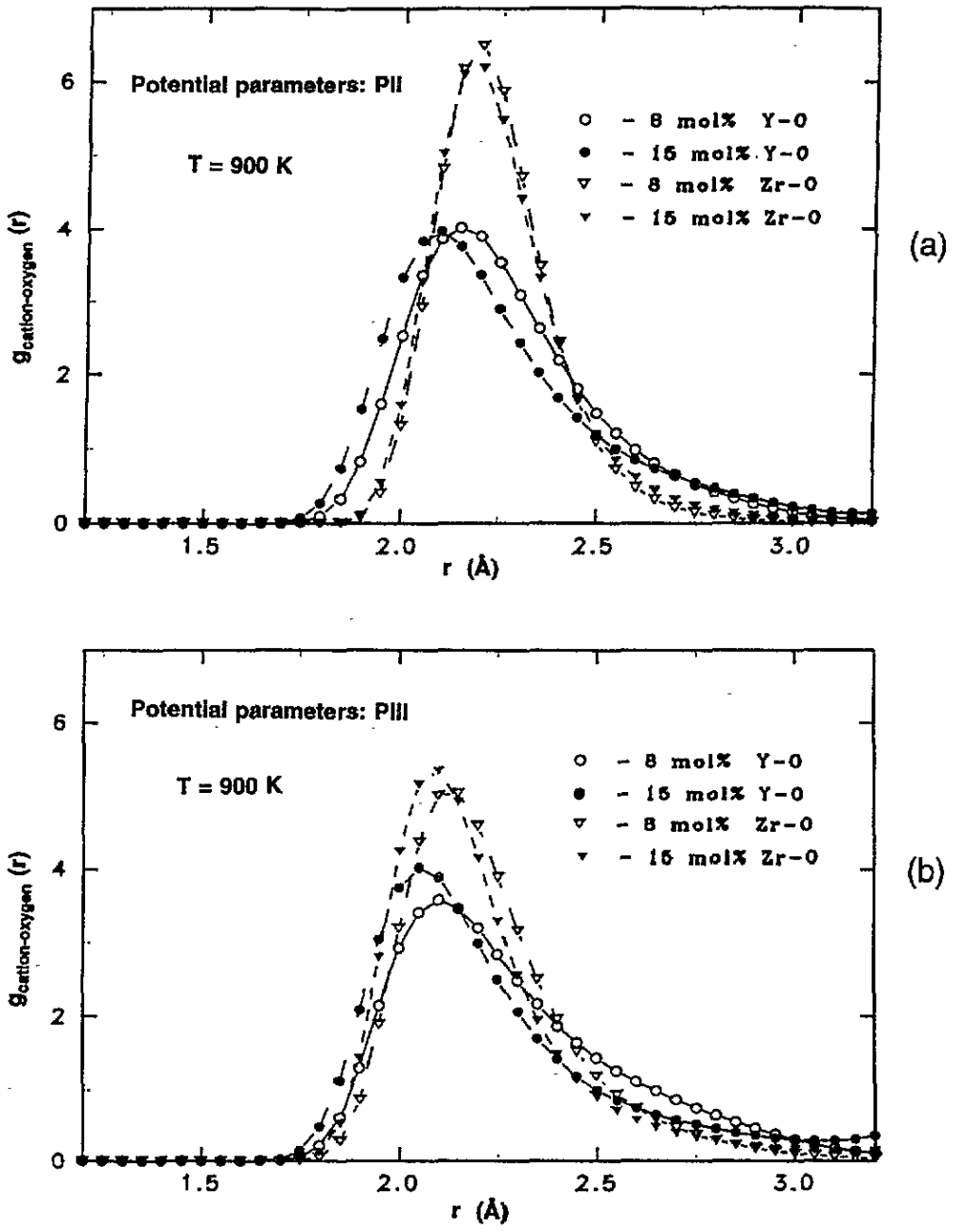

Figure 7. Radial distribution functions of Zr–O and Y–O pairs at 8.00 and 14.89 mol% Y_2O_3 with YI distribution and $T = 900$ K. (a) Potential PII. (b) Potential PIII.

displacements.

The extended x-ray absorption fine-structure results by Catlow *et al* (1986b) showed that oxygen vacancies are nearest neighbours of Zr^{4+} ions, and the local structural environment of Zr^{4+} ions is more disordered than the environment of Y^{3+} ions at low temperatures

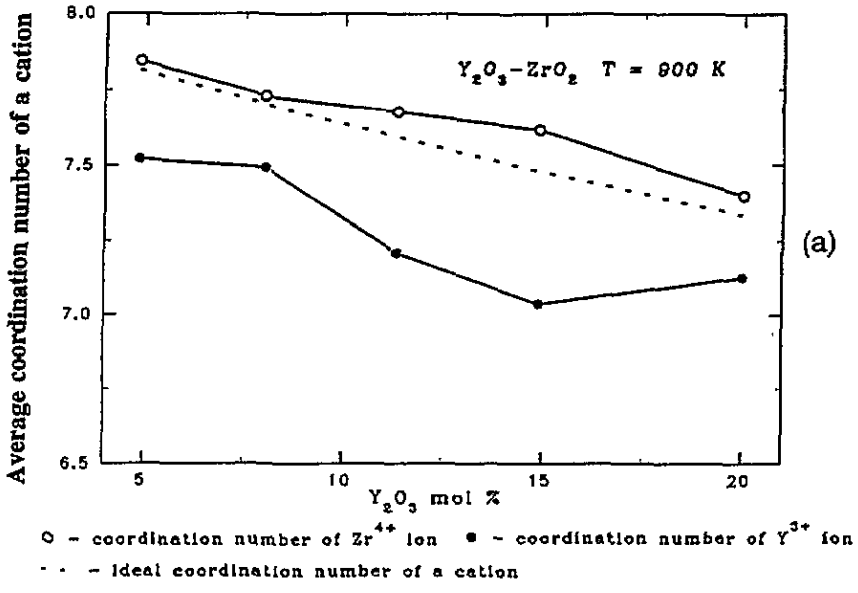

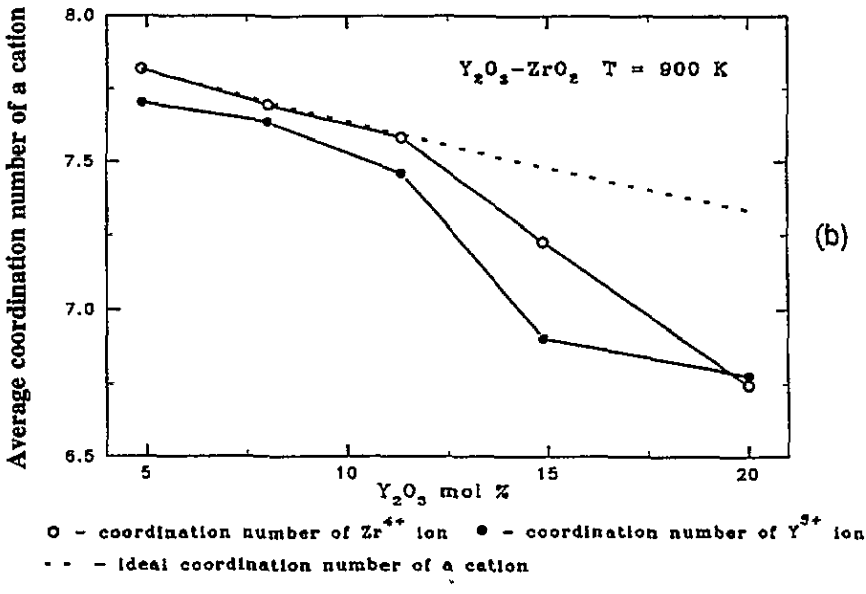

Figure 8. Coordination numbers of cations as function of Y_2O_3 concentration. Conditions: YI and $T = 900$ K. (a) Potential PII. (b) Potential PIII.

($T < 600$ K) for the 11.5 mol% Y_2O_3–ZrO_2 system. As the temperature increases, the local structural environments of the two cations are getting more alike. Atomistic calculations (Catlow *et al* 1986a) showed that it is energetically more favourable for an oxygen vacancy to be the nearest neighbour of a Zr^{4+} ion than of an Y^{3+} ion in the Y_2O_3–ZrO_2 system. Our simulation results seem to be contradictory to these results. Further experimental work in wider temperature and concentration ranges and more simulations may be needed in order

to resolve this.

In order to analyse the effect of Y–Y clusters on vacancy trapping, we classified the Y^{3+} and Zr^{4+} ions according to how many Y^{3+} ions there are in the nearest-neighbour (NN) positions. Then the average coordination number of oxygen around a cation for each class of the Y^{3+} or Zr^{4+} ions was calculated. These results are shown in figure 9 for 8.00 and 11.34 mol% Y_2O_3 with YII, PIII, and $T = 900$ K.

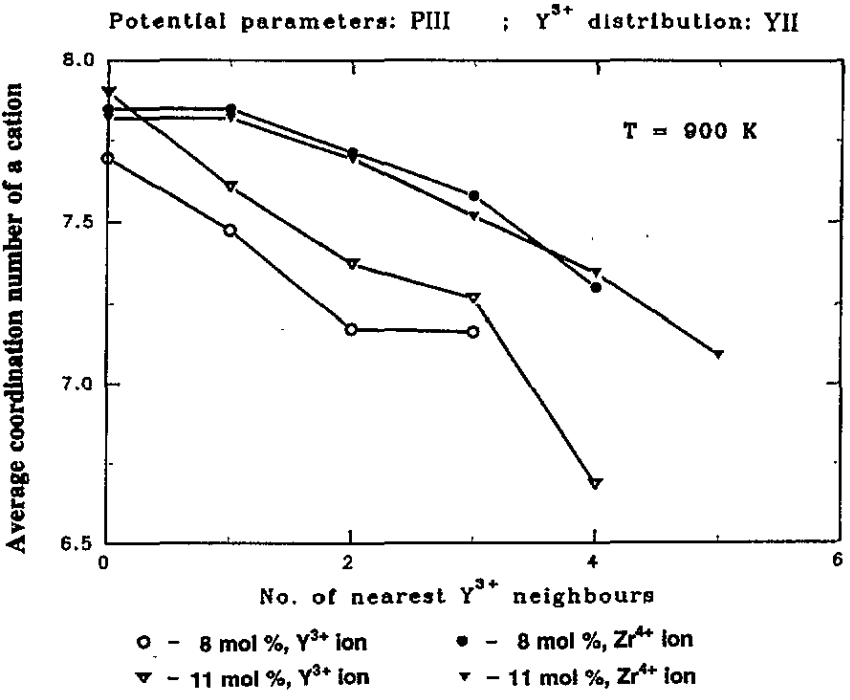

Figure 9. Coordination numbers of cations as function of the number of Y^{3+} ions in NN positions at 8.00 and 11.34 mol% Y_2O_3. Potential PIII.

When there are more Y^{3+} ions in the near neighbourhood, both Y^{3+} and Zr^{4+} ions have fewer oxygen ions around them. This result further confirms that NN Y–Y clusters trap oxygen vacancies. The bigger the Y–Y cluster is, the more vacancies will be trapped in the region.

Figure 10 shows the corresponding results for the 14.89 mol% Y_2O_3–ZrO_2 system with YI and YII distributions. Unlike in figure 9, the coordination numbers do not decrease monotonously with increasing number of nearest Y^{3+} neighbours. This is because the numbers of Y^{3+} ions in the NNN positions are large and the effects from NN and NNN clusters superpose on each other. This shows that the NNN Y–Y clusters also play an important role in trapping the oxygen vacancies at high Y_2O_3 concentrations.

5. Conclusions

By employing the rigid-ion potential model in MD simulations of the Y_2O_3–ZrO_2 system, we have shown that both potential parameters PII and PIII predict the isothermal conductivity

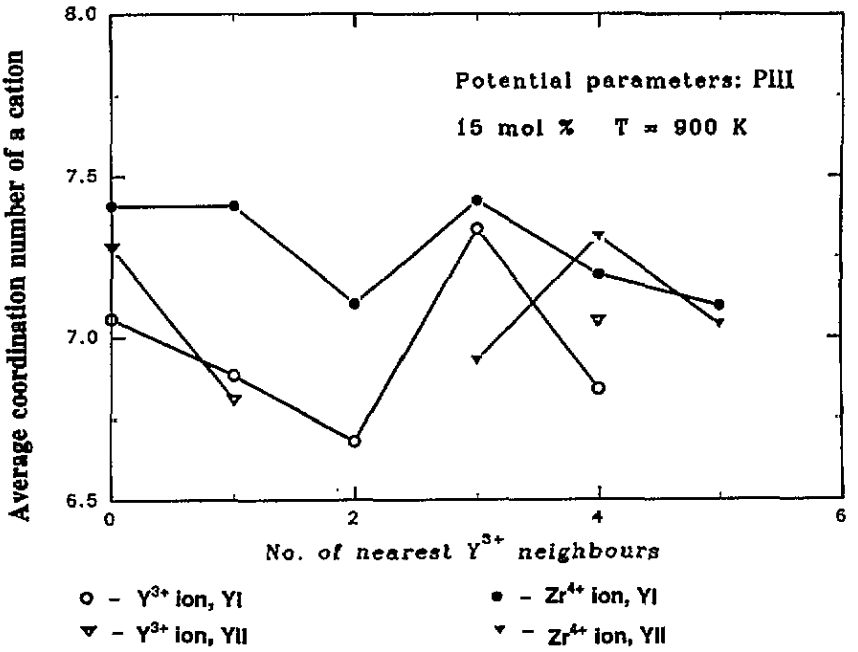

Figure 10. Coordination numbers of cations as function of the number of Y^{3+} ions in NN positions at 14.89 mol% Y_2O_3. Potential PIII.

maximum at low temperatures. Potential PIII leads to a more pronounced conductivity fall after the maximum. The dopant cation distribution has been found to influence the ionic conductivity. The ionic conductivity decreases with increasing number of nearest-Y–Y-neighbour pairs.

The oxygen ions are displaced about 0.37 Å towards O^{2-} vacancies. The local structural environment of Y^{3+} ions is more disordered than that of the Zr^{4+} ions. The Y^{3+} ions are found to have smaller coordination numbers than the Zr^{4+} ions, indicating that oxygen vacancies are nearest neighbours of Y^{3+} ions. The simulation results for the coordination numbers of cations strongly suggest that oxygen vacancies are trapped by the Y^{3+} ions in the Y_2O_3–ZrO_2 system.

The nearest- and next-nearest-neighbour Y–Y pairs can form clusters at high Y_2O_3 concentrations. The simulation results show that the bigger sizes the Y–Y neighbour clusters have, the more vacancies will they trap. As a consequence, the ionic conductivity will be decreased drastically.

To this end, we suggest that the increasing *numbers* and the *sizes* of the Y–Y clusters are responsible for the isothermal conductivity decrease at high Y_2O_3 concentrations in the Y_2O_3–ZrO_2 system.

Acknowledgments

We wish to thank Professor John Kincaid from the State University of New York at Stony Brook for many constructive discussions. The main FORTRAN code MDIONS was provided by Dr Fincham at the Computer Centre at the University of Keele. Financial support for this work was provided by NAVF (The Norwegian Research Council for Science and

Humanities, grant No 432.89/070) and an NTH (The Norwegian Institute of Technology) scholarship. NAVF has supported CPU time on the CRAY Y-MP supercomputer at RUNIT (Trondheim). Free computer time was also provided by the IBM cluster at USIT (University of Oslo).

References

Allen M P and Tildesley D J 1987 *Computer Simulation of Liquids* (Oxford: Clarendon)
Beeman D 1976 *J. Comput. Phys.* **20** 130–9
Bingham D, Tasker P W and Cormack A N 1989 *Phil. Mag.* A **60** 1–14
Butler V, Catlow C R A and Fender B E F 1981 *Solid State Ion.* 5 539–42
Casselton R E W 1970 *Phys. Status Solidi* a **2** 571–87
Catlow C R A 1984 *Solid State Ion.* **12** 67–73
Catlow C R A, Chadwick A V, Cormack A N, Greaves G N, Leslie M and Moroney L M 1986a *Mater. Res. Soc. Symp. Proc.* **60** 173–8
Catlow C R A, Chadwick A V, Greaves G N and Moroney L M 1986b *J. Am. Ceram. Soc.* **69** 272–7
Claussen N, Rühle M and Heuer A H 1984 *Science and Technology of Zirconia II (Advances in Ceramics 12)*
Cormack A N 1986 *Mater. Sci. Forum* **7** 177
Cormack A N and Catlow C R A 1985 *Transport in Nonstoichiometric Compounds (NATO ASI Series B 129)* ed G Simkovich and V S Stubican, pp 101–10
Dwivedi A and Cormack A N 1989 *J. Solid State Chem.* **79** 218–31
El Barhmi A, Schouler E J L, Hammou A and Kleitz M 1988 *Solid State Ion.* **28–30** 493–6
Fincham D 1982 *Comput. Phys. Commun.* **25** 159–76, 177–9
Heuer A H and Hobbs L W (ed) 1981 *Science and Technology of Zirconia (Advances in Ceramics 3)*
Hohnke D K 1979 *Fast Ion Transport in Solids* ed P Vashishta, J N Mundy and G K Shenoy (Amsterdam: North-Holland) pp 669–72
—— 1981 *Solid State Ion.* 5 531
Hudson B and Moseley P T 1976 *J. Solid State Chem.* **19** 383–9
Hull S, Farley T W D, Hackett M A, Hayes W, Osborn R, Andersen N H, Clausen K, Hutchings M T and Stirling W G 1988 *Solid State Ion.* **28–30** 488–92
Ingel R P and Lewis D III 1986 *J. Am. Ceram. Soc.* **69** 325–32
Li X 1993 Ion transport in solid electrolytes studied by molecular dynamics simulations *PhD Thesis* The Norwegian Institute of Technology, University of Trondheim
Mackrodt W C and Woodrow P M 1986 *J. Am. Ceram. Soc.* **69** 277–80
Morinaga M, Cohen J B and Faber J Jr 1979 *Acta Crystallogr.* A **35** 789–95
Murch G E, Murrey A D and Catlow C R A 1986 *Solid State Ion.* **18/19** 196
Nowick A S 1984 *Diffusion in Crystalline Solids* ed G E Murch and A S Nowick (Orlando: Academic) pp 143–88
Oishi Y and Ando K 1985 *Transport in Nonstoichiometric Compounds (NATO ASI Series B 129)* ed G Simovich and V S Stubican, pp 189–201
Park K and Olander D R 1991 *J. Electrochem. Soc.* **138** 1154–9
Poulsen F W, Andersen N H, Clausen K, Skaarup S and Sørensen O T (ed) 1985 *Transport-Structure Relations in Fast Ion and Mixed Conductors, Proc. 6th Risø Int. Symp. on Metallurgy and Matererials Science*
Simpson L A and Carter R E 1966 *J. Am. Ceram. Soc.* **49** 139
Sōmiya S, Yamamoto N and Yanagida H 1988 *Science and Technology of Zirconia III (Advances in Ceramics 24)*
Stoneham A M (ed) 1989 *Ionic Solids at High Temperatures* (Singapore: World Scientific)
Stubican V S 1988 *Science and Technology of Zirconia III (Advances in Ceramics 24)* ed S Sōmiya, N Yamamoto and H Yanagida, pp 71–82
Takahashi T (ed) 1989 *High Conductivity Solid Ionic Conductors, Recent Trends and Applications* (Singapore: World Scientific)
Vashishta P, Mundy J N and Shenoy G K (ed) 1979 *Fast Ion Transport in Solids* (Amsterdam: North-Holland)